Progress In Electromagnetics Research B, Vol. 56, 235–250, 2013

TIME-REVERSAL MICROWAVE IMAGING BASED ON RANDOM CONFIGURATION OF TRANSMITTERS OR RECEIVERS

Mojtaba Razavian, Mohammad H. Hosseini, and Reza Safian*

Department of Electrical and Computer Engineering, Isfahan University of Technology, Isfahan 84156-83111, Iran

Abstract—Imaging techniques based on time reversal method are particularly suitable for detection of targets embedded in a strongly scattering media. Generally in time reversal imaging technique we need to know the Green's function of the medium and the exact locations of the transmitter and receiver antennas. We introduce a target imaging method in which imaging is made with an arbitrary placement of the transmitting or receiving antennas. Numerical simulations are used to illustrate the capabilities of the proposed algorithms in different scenarios. We use the two-dimensional finite difference time domain method in our simulations. The numerical simulations are done for a typical through-the-wall scenario. We also present results in which the same method is used for tracking targets behind the wall.

1. INTRODUCTION

In sensing and imaging problems, the object is often concealed by a medium which obscures its relevant features. A possible candidate for probing the target may be a wave field (e.g., electromagnetic radiation), that travels through the medium and modified by the objects before being captured by means of sensors or detectors. Microwave signals can penetrate through foliage, fog and smoke to detect the hidden objects, and mm-waves can propagate inside walls, clothing and packaging. Due to these interesting capabilities of microwave and millimeter wave portion of electromagnetic spectrum compared to visible and infrared, they are excellent candidates for applications involving in detection, localization and classification of obscured targets. Ultra

Received 8 August 2013, Accepted 5 November 2013, Scheduled 7 November 2013

* Corresponding author: Reza Safian (rsafian@cc.iut.ac.ir).

wide-band (UWB) microwave signals are possible candidates to obtain a reasonable resolution and penetration simultaneously. In general, UWB radar systems are of great interest because they cover a variety of application fields including land mine detection, robotics, and security systems. In particular, surveillance systems have attracted much attention because they are of great importance in military and low enforcement missions.

A number of classical approaches such as Doppler processing and spatial beam-forming exist for radar surveillance and localization. But a new method, which utilizes UWB operation is time reversal (TR) technique introduced by Fink [1]. The TR technique is based on a fundamental symmetry of physics, i.e., the time reversal invariance [2]. In the TR operation, because of time reversal invariance in lossless media, signals emitted from a source can automatically be refocused on the original source location, when being captured and time reversed by a time reversal array. This property has been exploited in acoustics and more recently in electromagnetics [3], leading to a broad area of applications. It has been demonstrated that in an environment where multi-path scattering dominates focusing of acoustic waves with super resolution can be achieved using time-reversal method [4].

The basis of the time reversal method is application of the time reversal operator (TRO) to the sampled scattered fields. Eigenspace analysis of the TRO provides information about the scattering scenario under study. Specifically, in the case of multiple scatterers, selective focusing on the desired scatterers is possible via the decomposition of the TRO method (DORT under its French acronym) [5, 6]. Similarly, TR-MUSIC (Multiple signal Classification) method developed in [7] utilizes TRO to obtain TR-based imaging for the localization of target(s) [8].

Generally, time reversal method requires multiple antennas to form the multi-static matrix. This is not always easy to realize in practice, especially when transmitter and receiver antennas coincide. The main difficulty is the coupling between the transmitting and receiving antennas which influences the sampled scattered field. By separating the transmitter and the receiver antenna arrays we can avoid this problem. In [8], the DORT method and MUSIC algorithm are generalized to the case where the transmitter and receiver arrays do not coincide. But we need the information about the location of both receiver array and transmitter array which is not usually available specially in the case of through-the-wall imaging application. Here we show that it is possible to perform imaging knowing the location and the Green's function of only one of the transmitting or receiving arrays. This is very useful in cases such as TWI which we have limited access

the space where the target is located. The results are simulated using two dimensional finite difference time domain (FDTD) method in an isotropic medium and using a ultra-wideband pulse, first derivative of Blackman Harris, as the excitation of the transmitting antenna(s). Numerical results are presented for targets in free space and imaging and tracking of conducting targets are performed in the presence of a lossy wall.

2. TIME REVERSAL MUSIC METHOD WITH RANDOM TRANSMITTER ARRANGEMENT

The eigenvalue decomposition of the time reversal operator forms the basis for both TR-DORT and TR-MUSIC methods. These two approaches allow for TR-based imaging via the use of complementary subspaces of the time reversal operator. Specifically, DORT employs the signal subspace whereas TR-based MUSIC employs the null subspace. For well-resolved point-like scatterers, information on scatterer strengths and locations are partially encoded by the eigenvalues and associated eigenvectors of the time reversal operator signal subspace [8]. Back-propagation of these eigenvectors yields target images. However, DORT performance degrades if the well-resolvedness criterion is not met. This is due to the fact that the signal subspace eigenvectors become linear combinations of the Green's functions vectors connecting scatterers to the time reversal operator. Back-propagation of such signal subspace eigenvectors creates overlapped image fields which hinders target imaging and localization. On the other hand, regardless of the well-resolvedness criteria, the time reversal operator null subspace is orthogonal to its signal subspace, (i.e., projection of any vector formed by the linear combination of signal subspace eigenvectors onto the null subspace is (ideally) zero). This property is the basis of TR-based MUSIC method which provides better detection and localization properties than DORT even for poorly-resolved scatterers (assuming homogeneous media). TR-based MUSIC was first considered in [7] assuming Born approximation and coincident arrays and later extended to more general array configurations [8]. Here we have used the TR-based MUSIC method in our imaging examples.

A general imaging scenario is shown in Fig. 1. Receivers are marked as circles and transmitters as squares. The cross shows the location of the target (in general we can have several targets) and the triangles are the locations of the clutter objects. Each arrow identifies the Green's function between a transmitter and a target or a receiver and a target. Let N_t and N_r be the numbers of transmitters

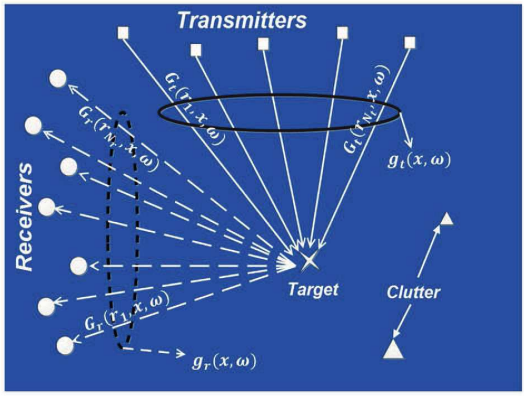

Figure 1. Transmitting and receiving antenna positions. The squares are transmitting antennas and the circles are receiving antennas that are placed randomly.

and receivers respectively (Fig. 1). Based on the basic time reversal theory higher number of transmitter or receivers increases the imaging resolution. The multi-static data matrix $\mathbf{K}$ is a $N_r \times N_t$ matrix where $k_{ij}(t)$ corresponds to the signal received at the ith antenna when a short pulse $s(t)$ is transmitted from the jth antenna as the sole transmitter. The Fourier transform of $\mathbf{K}(t)$ yields $\mathbf{K}(\omega) = [k_{ij}(\omega)]$ for $\omega \in \Omega_s$, where Ω_s is the frequency bandwidth of operation. For point-like and well-resolved scatterers multi-static data matrix (MDM) is defined as [9],

$$\mathbf{K}(\omega) = [k_{ij}(\omega)]_{N_r \times N_t}, \tag{1}$$

where,

$$k_{ij}(\omega) = S(\omega) \sum_{m=1}^{M} \tau_m(\omega) G_r(r_i, x_m, \omega) G_t(r_j, x_m, \omega), \tag{2}$$

and $S(\omega)$ is the transmitted signal in frequency domain. $\tau_m(\omega)$ is the scattering coefficient of mth scatterer and M is the total number of scatterers. $G_r(r_i, x_m, \omega)$ and $G_t(r_j, x_m, \omega)$ are Green's functions of medium between receiver/transmitter array antenna and the target, respectively. r_i and r_j are the locations of ith and jth antennas, respectively and x_m is the location of mth scatterer. We can write the MDM matrix in another form as,

$$\mathbf{K}(\omega) = S(\omega) \sum_{m=1}^{M} \tau_m(\omega) \mathbf{g}_r(x_m, \omega) \mathbf{g}_t^{\mathrm{T}}(x_m, \omega), \tag{3}$$

where,

$$\mathbf{g}_r(x_m,\omega) = [G_r(r_1,x_m,\omega),\ldots,G_r(r_{N_r},x_m,\omega)]^{\mathrm{T}}, \quad (4)$$

$$\mathbf{g}_t(x_m,\omega) = [G_t(r_1,x_m,\omega),\ldots,G_t(r_{N_t},x_m,\omega)]^{\mathrm{T}} \quad (5)$$

are steering vectors of receiver and transmitter array antennas respectively. Here T represents the matrix transpose operation. Now we can define the operating matrices $\mathbf{T}$ and $\mathbf{L}$ as

$$\mathbf{T} = \mathbf{K}^{\dagger}\mathbf{K} = |S(\omega)|^2 \sum_{m=1}^{M} |\tau_m(\omega)|^2 \times \mathbf{g}_t{}^{*}(x_m,\omega)\mathbf{g}_r{}^{\dagger}(x_m,\omega)\mathbf{g}_r(x_m,\omega)\mathbf{g}_t{}^{\mathrm{T}}(x_m,\omega), \quad (6)$$

$$\mathbf{L} = \mathbf{K}\mathbf{K}^{\dagger} = |S(\omega)|^2 \sum_{m=1}^{M} |\tau_m(\omega)|^2 \times \mathbf{g}_r(x_m,\omega)\mathbf{g}_t{}^{\mathrm{T}}(x_m,\omega)\mathbf{g}_t{}^{*}(x_m,\omega)\mathbf{g}_r{}^{\dagger}(x_m,\omega), \quad (7)$$

where $*$ represents the complex conjugation, and $\dagger$ represents the hermitian conjugate. For imaging we need to calculate the eignevectors and associated eigenvalues of $\mathbf{T}$ and $\mathbf{L}$ as $\{\mathbf{e}_j,\lambda_j\}_{1<j<N_t}$ and $\{\mathbf{V}_j,\sigma_j\}_{1<j<N_r}$ respectively.

As the well-resolvedness criterion for the scatterers is weakened, signal subspace eigenvectors become linear combinations of the Green's function vectors connecting the scatterers to the time reversal array [8]. As a result, imaging using these eigenvectors creates interferences that degrades the scatterer location estimates. However, even for closely-spaced scatterers, null subspace is still orthogonal to the signal subspace. Therefore, inner products of the steering vectors with the null subspace eigenvectors would vanish only at the scatterer location(s) which can provide a good imaging functional. This forms the basis for the TR-based MUSIC, where the imaging functional (pseudo-spectrum) function at an arbitrary test point X_p is originally defined as [8],

$$H(X_p) = \frac{1}{\sum_j \left[|\mathbf{e}_j{}^{\mathrm{T}}\mathbf{g}_t(X_p)| + \left|\mathbf{V}_j{}^{\dagger}\mathbf{g}_r(X_p)\right|\right]} \quad (8)$$

where $\mathbf{e}_j$ and $\mathbf{V}_j$ are eigenvectors associated with eigenvalues smaller than a certain threshold and

$$j \le \min(N_r, N_t) \quad (9)$$

and $\mathbf{g}_t(X_p) = \{\mathbf{g}_{t_i}(X_p)\}_{(1\le i\le N_t)}$ is the Green's function vector of the transmitting array and $\mathbf{g}_r(X_p) = \{\mathbf{g}_{r_i}(X_p)\}_{(1\le i\le N_r)}$ is the Green's

function vector of the receiving array at the test point X_p. The function $H(X_p)$ peaks at the scatterer locations. It is worth mentioning that the constraint $j \leq \min(N_t, N_r)$ in the summation is not necessary and we can use all the eigenvectors corresponding to small eigenvalues.

To better understand the pseudo-spectrum function we have expanded the operating matrices $\mathbf{T}$ and $\mathbf{L}$. The products ${\mathbf{g}_r}^{\dagger}(x_m,\omega)\mathbf{g}_r(x_m,\omega)$ and ${\mathbf{g}_t}^{\mathrm{T}}(x_m,\omega)\mathbf{g}_t{}^*(x_m,\omega)$ in Equations (6) and (7) can be written as

$$\begin{aligned} &{\mathbf{g}_r}^{\dagger}(x_m,\omega)\mathbf{g}_r(x_m,\omega) \\ &= \|\mathbf{g}_r(x_m,\omega)\|^2 = \left\{|G_r(r_1,x_m,\omega)|^2 + \ldots + |G_r(r_{N_r},x_m,\omega)|^2\right\} \end{aligned} \tag{10}$$

and

$$\begin{aligned} &{\mathbf{g}_t}^{\mathrm{T}}(x_m,\omega)\mathbf{g}_t{}^*(x_m,\omega) \\ &= \|\mathbf{g}_t(x_m,\omega)\|^2 = \left\{|G_t(r_1,x_m,\omega)|^2 + \ldots + |G_t(r_{N_t},x_m,\omega)|^2\right\} \end{aligned} \tag{11}$$

Hence the operating matrices $\mathbf{T}$ and $\mathbf{L}$ can now be reformed as,

$$\mathbf{T} = \mathbf{K}^{\dagger}\mathbf{K} = |S(\omega)|^2 \sum_{m=1}^{M} |\tau_m(\omega)|^2 \|\mathbf{g}_r(x_m,\omega)\|^2 \times \underbrace{\begin{pmatrix}\boldsymbol{\Psi}_1 & \ldots & \boldsymbol{\Psi}_{N_t}\end{pmatrix}}_{\Lambda} \tag{12}$$

and

$$\mathbf{L} = \mathbf{K}\mathbf{K}^{\dagger} = |S(\omega)|^2 \sum_{m=1}^{M} |\tau_m(\omega)|^2 \|\mathbf{g}_t(x_m,\omega)\|^2 \times \underbrace{\begin{pmatrix}\boldsymbol{\Psi}'_1 & \ldots & \boldsymbol{\Psi}'_{N_r}\end{pmatrix}}_{\Lambda'} \tag{13}$$

where

$$\boldsymbol{\Psi}_i = \begin{pmatrix} G_t(r_1,x_m,\omega)^* G_t(r_i,x_m,\omega) \\ \vdots \\ G_t(r_{N_t},x_m,\omega)^* G_t(r_i,x_m,\omega) \end{pmatrix} \tag{14}$$

$$\boldsymbol{\Psi}'_j = \begin{pmatrix} G_r(r_1,x_m,\omega) G_r(r_j,x_m,\omega)^* \\ \vdots \\ G_r(r_{N_r},x_m,\omega) G_r(r_j,x_m,\omega)^* \end{pmatrix} \tag{15}$$

It can be seen that $\boldsymbol{\Lambda}$ and $\boldsymbol{\Lambda}'$ in $\mathbf{T}$ and $\mathbf{L}$ are only in terms of the Green's functions of transmitting array and receiving array respectively. Therefore, we can define the imaging functional based on the matrix part of the $\mathbf{T}$ or $\mathbf{L}$. Here we have defined the imaging functional based on $\mathbf{L}$ which is more suitable for through-the-wall imaging applications as it will be explained later. The imaging functional is defined as

$$H(X_p) = \frac{1}{\sum_j \left|{\mathbf{V}_j}^{\dagger}\mathbf{g}_r(X_p)\right|} \tag{16}$$

It means that we can make imaging by knowing only one Green's function of receiver array. In other words, it is enough to know only the location of receiver array antenna for constructing the image.

In our first example we use a two dimensional finite difference time domain code with $N_x \times N_y = 200 \times 250$ grid points. The space discretization is uniform with $\Delta_x = \Delta_y = \Delta = 1\,\text{cm}$. The excitation is a TM_z electromagnetic wave with E_z, H_x, and H_y components. Each of the isolated dipole sources is z-directed (J_z) and the transmitting linear array antennas is along a line parallel to the x-axis. The receiving antenna array consists of z-oriented dipoles placed in random positions along a line perpendicular to transmitting array antennas. The transmitting antenna array consists of $N_t = 4$ antennas and the receiving antenna array consists of $N_r = 7$ antennas. The medium is lossless and isotropic. The excitation of the transmitting antennas, $S(t)$, is an ultra-wideband time-domain excitation. It is the first derivative of the Blackman-Harris (BH) pulse that vanishes after a time period of $T = 1/f_c$, where $f_c = 400\,\text{MHz}$ is the central frequency (Fig. 2). There are two cylindrical perfect electric conductor targets in the medium with different radii $r_1 = 2\,\text{cm}$ and $r_2 = 3\,\text{cm}$. They are placed at $(X_1, Y_1) = (60, 30)\,\text{cm}$, and $(X_2, Y_2) = (130, 50)\,\text{cm}$, respectively. The computational setup is shown in Fig. 1 where squares show the locations of transmitters, circles show the locations of receivers, crosses show the locations of the objects, and triangles show the locations of the clutter objects. First we form the **T** and **L**

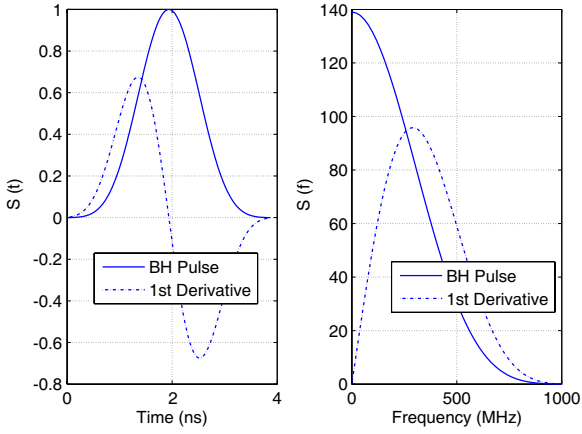

Figure 2. (a) Blackman Harris pulse. (b) Fourier transform of the Blackman Haarris pulse.

matrices for the two cylindrical targets in the absence of clutter objects. Eigenvalues are obtained by applying eigenvalue decomposition to these matrices. The first four eigenvalues of **T** and **L** matrices are plotted in Fig. 3. The eigenvalues are normalized with respect to their maximum in order to compare their frequency distribution. The 1st eigenvalue of both matrices has two peaks because of multiple reflections between the two scatterers in the medium. The second eigenvalue has only one peak. It is due to the time limit of the experiment which removes the multiple scattering of the 2nd scatterer. The 3rd and 4th eigenvalues distribution is similar to the 2nd one. But note that their frequency distribution are outside of the first and second eigenvalue frequency distribution and can not be of another scatterer. The last three eigenvalues of the matrix **L** have near zero fluctuating distributions.

Figure 4 shows the images of the targets where both transmitting and receiving steering vectors are used. Figs. 5 and 6 show the same image using only receiving and transmitting steering vectors, respectively. As can be seen from these images, having the steering vector of receiving array is sufficient for detection of the targets. Same results are obtained by using only the steering vector of transmitting array if $H(X_p)$ is properly defined. Based on our simulations the introduced technique also works in the case the objects are larger than a wavelength.

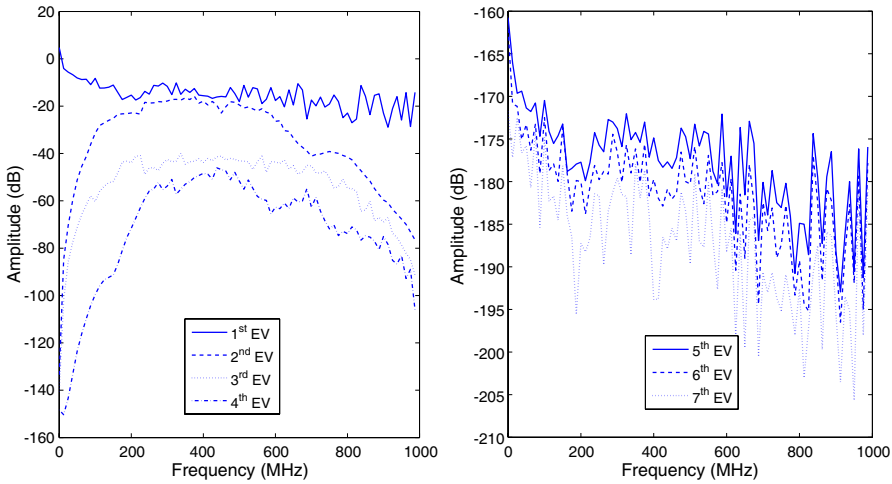

Figure 3. (a) The first four normalized eigenvalue (EV) frequency distribution of matrix **L**. (b) The first four normalized eigenvalue (EV) frequency distribution of matrix **T**.

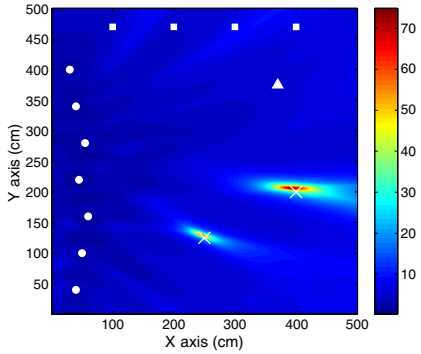

Figure 4. Imaging using only receiving steering vector.

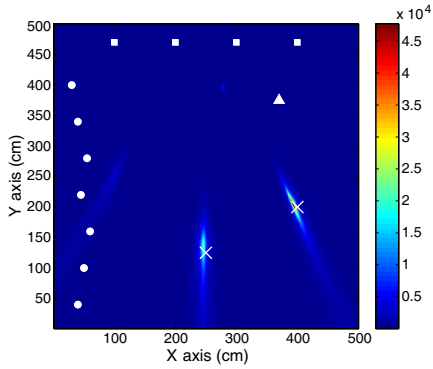

Figure 5. Imaging using only transmitting steering vector.

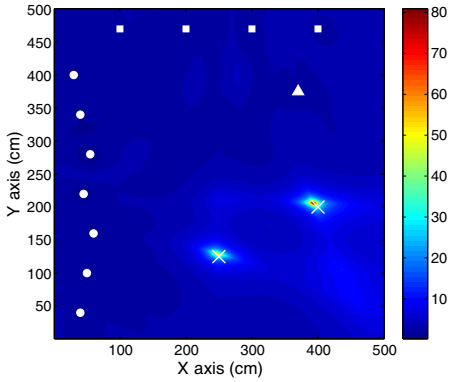

Figure 6. Imaging using both steering vectors.

3. THROUGH-THE-WALL IMAGING AND TARGET TRACKING WITH RANDOM TRANSMITTER ARRANGEMENT

For through-the-wall imaging (TWI), one needs to know not only if there is any target behind the wall but also where the target is located. Previously, several effective TWI algorithms have been proposed to address this problem [10–12]. In this paper, we focus on TWI within the framework of time reversal. In particular, the TR-MUSIC method is employed for target detection and localization and tracking behind the wall. Through-the-wall imaging is one of the toughest scenarios in microwave imaging therefore it is a good

benchmark for the introduced method and shows that it is effective. On the other hand in realistic through-the-wall imaging applications the space behind the wall is generally not accessible. Therefore the possibility of exploiting preexisting transmitting antennas which are placed in random locations for imaging is very interesting. For example WiFi antennas which are already installed in the room, behind the wall, at unknown location are used as transmitters and transmitted signal is received using an antenna array in front of the wall. Hence, imaging is done only knowing the location of the receiving array antennas.

In our first example of through-the-wall imaging there are two point-like static cylindrical conductor objects in the room at locations $x_{m_1} = (90, 70)\,\text{cm}$ and $x_{m_2} = (130, 55)\,\text{cm}$ with radii $R_1 = 3\,\text{cm}$ and $R_2 = 2\,\text{cm}$. We consider a uniform linear array of 7 elements centered at the position r_j at a distance of 15 cm in front of the wall, where, $j = 1, 2, \ldots, 7$, $r_j = (x_j, y_j)$. The receiver antenna elements are placed with an inter-element spacing $\Delta_x = 20\,\text{cm}$ and $r_1 = (x_1, y_1) = (41, 15)\,\text{cm}$. The two transmitting antennas are placed randomly in room which in the first simulation are in positions, $(x_1, y_1) = (41, 226)\,\text{cm}$ and $(x_2, y_2) = (121, 226)\,\text{cm}$ and in the second simulation are in positions, $(x_1, y_1) = (70, 220)\,\text{cm}$ and $(x_2, y_2) = (100, 90)\,\text{cm}$. The wall is homogeneous with parameters, $\varepsilon_r = 3$ and $\sigma = 0.02\,\text{S/m}$, and thickness, $d = 5\,\text{cm}$. Fig. 7 shows the images of two cylindrical conducting targets which are located at random locations. Squares show the locations of transmitters, circles show the locations of receivers and, crosses show the locations of the objects. As it can been seen from the results random variation of the transmitter locations does

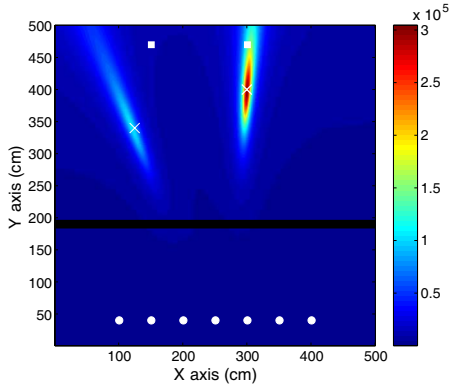

Figure 7. Through-the-wall imaging using two transmitting antennas at arbitrary locations. The solid line shows the location of the wall.

not deteriorates the image. In another example the target is moving in the space behind the wall. Using the transmitting antennas inside the room the movement path of target can be determined. The aim of the tracking algorithm is to enhance the contribution of moving target in the eigen-spectrum while suppressing that of stationary target. The procedure used here is based on differential MDM. At different instants of the target movement we record the MDM. Then for imaging and tracking the target two subsequent MDMs are subtracted from each other. Since the displacement of target movements between different snapshots is assumed much shorter than the wavelength ($\lambda = 30\,\text{cm}$) most of the contribution from stationary target and multiple scattering among target movements and stationary target cancel out. Thus, the eigen-spectrum of the differential MDM will mostly correspond to the target movements [13]. Here we record the waves, coming out from the antenna located at unknown locations using receiving antenna array behind the wall. At first there is no stationary target in room, and only a metal object moving across the room. We calculate the MDM at five different snapshots of moving metal at locations, $(x_1, y_1) = (40, 40), (x_2, y_2) = (60, 60), \ldots, (x_5, y_5) = (120, 120)\,\text{cm}$. Since there is no static object in this case we don't need differential MDMs and by using different MDMs, the target location can be determined. Fig. 8 shows the location of moving target at different snapshots.

In another TWI example we introduce a static metal box as a clutter object in the computational domain. To have an accurate point-like image of the moving target in the presence of clutter object,

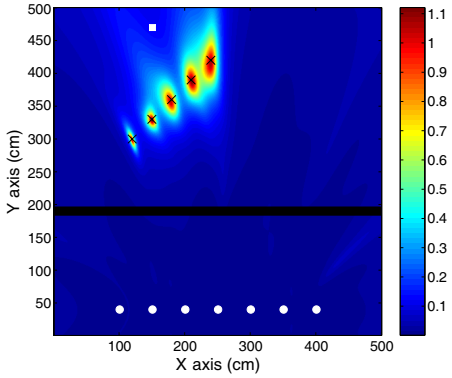

Figure 8. The crosses show the target locations. There is no stationary target in the room. The solid line shows the location of the wall.

we have to use the differential MDM approach. Traditionally [13], the differential MDM approach is implemented by subtracting the MDMs at two consecutive snapshots of the moving object as $\mathbf{K}_d(\omega) = \mathbf{K}_{i+1}(\omega) - \mathbf{K}_i(\omega)$, then using $\mathbf{K}_d(\omega)$ to calculate the operating matrix $\mathbf{L} = \mathbf{K}_d\mathbf{K}_d^{\dagger}$. In this case there will be only one non-zero eigenvalue for the $\mathbf{L}$ Matrix. This non-zero eigenvalue corresponds to target movement and the effect of stationary target is washed out due to destructive interference. Therefore,

$$\mathbf{K}_d(\omega) = \mathbf{K}_{i+1}(\omega) - \mathbf{K}_i(\omega) = S(\omega) \sum_{m=1}^{M} \tau_m(\omega) \times \left[\mathbf{g}_r(x_{m_{i+1}}, \omega)\mathbf{g}_t{}^{\mathrm{T}}(x_{m_{i+1}}, \omega) - \mathbf{g}_r(x_{m_i}, \omega)\mathbf{g}_t{}^{\mathrm{T}}(x_{m_i}, \omega)\right] \quad (17)$$

where $x_{m_{i+1}}$ is the current location of the mth target and x_{m_i} is the previous location of the mth target. We use the $\mathbf{K}_d(\omega)$ to calculate the $\mathbf{L}$ matrix as,

$$\begin{aligned}\mathbf{L} \;=\; |S|^2 \sum_{m=1}^{M} |\tau_m|^2 \Big[& \|\mathbf{g}_t(x_{m_{i+1}})\|^2 \mathbf{g}_r(x_{m_{i+1}})\mathbf{g}_r{}^{\dagger}(x_{m_{i+1}}) \\ & + \|\mathbf{g}_t(x_{m_i})\|^2 \mathbf{g}_r(x_{m_i})\mathbf{g}_r{}^{\dagger}(x_{m_i}) \\ & - \mathbf{g}_r(x_{m_{i+1}})\mathbf{g}_t{}^{\mathrm{T}}(x_{m_{i+1}})\mathbf{g}_t{}^{*}(x_{m_i})\mathbf{g}_r{}^{\dagger}(x_{m_i}) \\ & - \mathbf{g}_r(x_{m_i})\mathbf{g}_t{}^{\mathrm{T}}(x_{m_i})\mathbf{g}_t{}^{*}(x_{m_{i+1}})\mathbf{g}_r{}^{\dagger}(x_{m_{i+1}})\Big] \end{aligned} \quad (18)$$

Since the displacement is much shorter than a wavelength, the magnitude of the Green's function does not change significantly and only the changes in angles have to be considered. Then the steering vectors in two consecutive positions can be written as,

$$\begin{aligned}\mathbf{g}_r(x_{m_i}) \;&\simeq\; \mathbf{g}_r(x_{m_{i+1}}) \cdot e^{j\mathbf{\Phi}} \\ \mathbf{g}_t(x_{m_i}) \;&\simeq\; \mathbf{g}_t(x_{m_{i+1}}) \cdot e^{j\mathbf{\Theta}}\end{aligned} \quad (19)$$

For simplicity we write $\mathbf{g}(x_m)$ instead of $\mathbf{g}(x_m, \omega)$. The angle vectors $\mathbf{\Phi}$ and $\mathbf{\Theta}$ are $N_r \times 1$ and $N_t \times 1$ matrices, where each element is the phase difference of reciever/transmitter Green's functions due to target movement. If we use Equation (19) in Equation (18) we can write the $\mathbf{L}$ matrix as,

$$\begin{aligned}\mathbf{L} = |S|^2 \sum_{m=1}^{M} |\tau_m|^2 \mathbf{g}_r(x_{m_{i+1}})\mathbf{g}_r{}^{\dagger}(x_{m_{i+1}}) \cdot \Big[& \|\mathbf{g}_t(x_{m_{i+1}})\|^2 \mathbf{I}_{N_r \times N_r} \\ & + \|\mathbf{g}_t(x_{m_{i+1}})\|^2 \left(e^{j\mathbf{\Phi}} e^{-j\mathbf{\Phi}^{\mathrm{T}}}\right) - \left[\left(|\mathbf{g}_t(x_{m_{i+1}})|^2\right)^{\mathrm{T}} e^{j\mathbf{\Theta}^{\mathrm{T}}}\right]^{*} \left(e^{j\mathbf{\Phi}} \mathbf{I}_{1\times N_r}\right)^{\dagger} \\ & - \left[\left(|\mathbf{g}_t(x_{m_{i+1}})|^2\right)^{\mathrm{T}} e^{j\mathbf{\Theta}^{\mathrm{T}}}\right] \left(e^{j\mathbf{\Phi}} \mathbf{I}_{1\times N_r}\right)\end{aligned} \quad (20)$$

where $\|\mathbf{g}_t(x_{m_{i+1}})\|$ is the norm of the steering vector and $|\cdot|$ is an operator which compute the absolute value of each element of the vector. In the case of one transmitter it is calculated as,

$$\left(|\mathbf{g}_t(x_{m_{i+1}})|^2\right)^{\mathrm{T}} = \|\mathbf{g}_t(x_{m_{i+1}})\|^2 \tag{21}$$

$\mathbf{I}_{m\times n}$ is a matrix where each element is equals one. If we use only one transmitting antenna in the room the location of the target can be determined, but not exactly as a point like location as we had in the previous example. Fig. 9 shows a snapshot of the moving target. The location of stationary target is $(x, y) = (40, 70)$ cm and the first location of moving target is at $(x, y) = (100, 90)$ cm. The location of the transmitting antenna is at $(81, 226)$ cm and the location of receiving array antennas and the wall are the same as before. If we use two antennas instead of one, the location of the target will be a point like image.

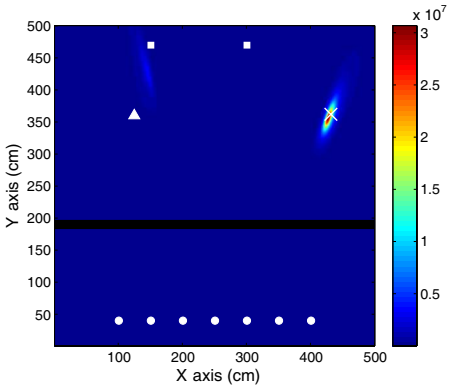

Figure 9. Target location at the fifth snapshot.

An alternative way to solve the tracking problem is to calculate two matrices, $\mathbf{L}_{i+1} = \mathbf{K}_{i+1}\mathbf{K}_{i+1}^{\dagger}$ and $\mathbf{L}_i = \mathbf{K}_i\mathbf{K}_i{}^{\dagger}$ at two consecutive locations of the target. Then construct a new matrix as $\mathbf{L}_d = \mathbf{L}_{i+1} - \mathbf{L}_i$. Therefore we will have two nonzero eigenvalue which correspond to moving target and the stationary clutter. It means that the effect of stationary clutter remains. Hence, the number of transmitting antennas must be at least as the same of total number of targets in the medium and we are able to find the location of both the moving and stationary targets in one simulation. To do this we have to calculate $\mathbf{L}_d$ as,

$$\mathbf{L} = \mathbf{L}_{i+1} - \mathbf{L}_i = |S|^2 \sum_{m=1}^{M} |\tau_m|^2 \|\mathbf{g}_t(x_{m_i})\|^2$$

$$\times \mathbf{g}_r(x_{m_{i+1}})\mathbf{g}_r{}^{\dagger}(x_{m_{i+1}}) \left[\mathbf{I}_{N_r \times N_r} - e^{j\mathbf{\Phi}} e^{-j\mathbf{\Phi}^{\mathrm{T}}}\right] \tag{22}$$

Figure 10 is an example with one moving target and a static clutter of this scenario in the room behind the wall. We have used two antennas located at arbitrary points. Fig. 11 shows the location of the moving target at different snapshots as red crosses.

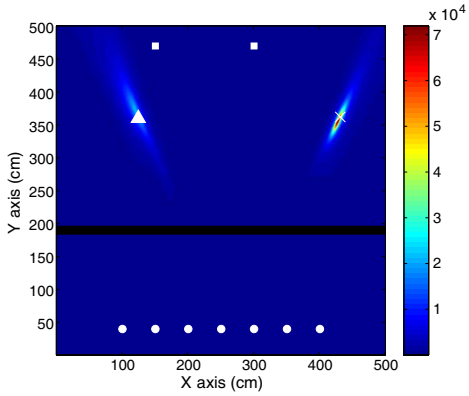

Figure 10. Location of stationary target and moving target using $\mathbf{L} = \mathbf{L}_8 - \mathbf{L}_7$ at seventh and eighth snapshots.

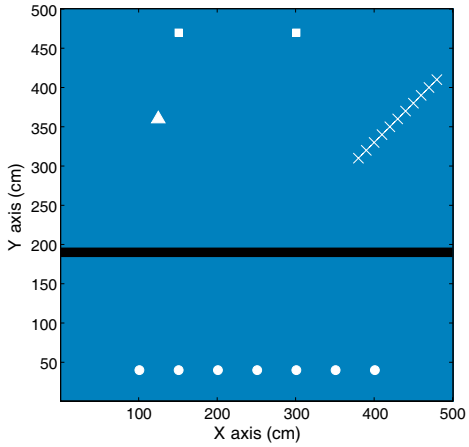

Figure 11. Final tracking path of the target behind the wall. The crosses show the metal locations and the square shows transmitting antenna and the circles show the receiving array antennas. The rectangle is the clutter.

4. CONCLUSION

In this paper we have used the MUSIC method for time reversal imaging. Based on the presented formulation for imaging we do not need to use the steering vector of both the transmitting and receiving arrays. By knowing the location of one of the arrays we can make imaging and find the location of targets. The only limitation here is that the number of transmitters must be at least as the number of targets in the medium. We have used the presented method to perform imaging in a through-the-wall scenario for static and moving targets. Two formulations for target tracking are presented. In one case, we are only able to locate the approximate moving object location with lower computational load. Using the other formulation, we are able to detect both static and moving targets at the same time with higher computational load.

REFERENCES

1. Fink, M., D. Cassereau, A. Derode, C. Prada, P. Roux, M. Tanter, J. L. Thomas, and F. Wu, "Time-reversed acoustics," *Rep. Prog. Physics*, Vol. 63, 1933–1995, 2000.
2. Dmitriev, V. A., "Space-time reversal symmetry properties of electromagnetic Green's tensor for complex and bianisotropic media," *Progress In Electromagnetics Research*, Vol. 48, 145–184, 2004.
3. Lerosey, G., J. De Rosney, A. Tourin, A. Derode, G. Montaldo, and M. Fink, "Time reversal of electromagnetic waves," *Phys. Rev. Lett.*, Vol. 92, 193904, 2004.
4. Bellomo, L., S. Pioch, M. Saillard, and E. Spano, "Time reversal experiments in the microwave range: Description of the radar and results," *Progress In Electromagnetics Research*, Vol. 104, 427–448, 2010.
5. Prada, C. and M. Fink, "Eigenmodes of the time reversal operator: A solution to selective focusing in multiple-target media," *Wave Motion*, Vol. 20, 151–163, 1994.
6. Prada, C., S. Manneville, D. Spoliansky, and M. Fink, "Decomposition of the time reversal operator: Detection and selective focusing on two scatterers," *J. Acoust. Soc. Am.*, Vol. 99, No. 4, 2067–2076, 1996.
7. Lev-Ari, H. and A. J. Devaney, "The time-reversal technique re-interpreted: Subspace-based signal processing for multi-static

target location," *Proceedings of the IEEE Sensor Array and Multichannel Signal Processing Workshop*, 509–513, 2000.

8. Lehman, S. K. and A. J. Devaney, "Transmission mode time-reversal super resolution imaging," *J. Acoust. Soc. Am.*, Vol. 113, 2742–2753, 2003.
9. Yavuz, M. E., "Time reversal based signal processing techniques for ultrawideband electromagnetic sensing in random media," Ph.D. Dissertation, Ohio State University, 2008.
10. Zhang, W., A. Hoorfar, and L. Li, "Through-the-wall target localization with time reversal music method," *Progress In Electromagnetics Research*, Vol. 106, 75–89, 2010.
11. Zhang, C. T. W., A. Hoorfar, and F. Ahmad, "Full polarimetric beam-forming algorithm for through-the-wall radar imaging," *Radio Science*, Vol. 46, 2011.
12. Zhang, W. and A. Hoorfar, "Two dimensional diffraction tomographic algorithm for through-wall radar imaging," *Progress In Electromagnetics Research B*, Vol. 31, 205–218, 2011.
13. Fouda, A. E. and F. L. Teixeira, "Imaging and tracking of targets in clutter using differential time-reversal techniques," *Waves in Random and Complex Media*, Vol. 22, No. 1, 66–108, 2012.